Electrocatalytic Hydrogen Evolution Reaction by a Ni(N₂O₂) Complex Based on 2,2'-bipyridine

Julia M. Dressel, Emma N. Cook, Shelby L. Hooe, Juan J. Moreno, Diane A. Dickie, and Charles W. Machan*

* - machan@virginia.edu; ORCID 0000-0002-5182-1138

JMD ORCID: 0000-0002-3601-9710; ENC ORCID: 0000-0002-0568-3600; SLH ORCID: 0000-0002-6991-2273; JJM ORCID: 0000-0003-1809-6170; DAD ORCID: 0000-0003-0939-3309

a – Department of Chemistry, University of Virginia, PO Box 400319, Charlottesville, VA 22904-4319

Abstract

In the face of rising atmospheric carbon dioxide (CO₂) emissions from fossil fuel combustion, the hydrogen evolution reaction (HER) continues to attract attention as a method for generating a carbon-neutral energy source for use in fuel cells. Since some of the best-known catalysts use precious metals like platinum, which have low natural abundance and high cost, developing efficient Earth abundant transition metal catalysts for HER is an important objective. Building off previous work with transition metal catalysts bearing 2,2'-bipyridine-based ligand frameworks, this work reports the electrochemical analysis of a molecular nickel(II) complex, which can act as an electrocatalyst for the HER with a Faradaic efficiency for H_2 of $94 \pm 8\%$ and turnover frequencies of 103 ± 6 s⁻¹ when pentafluorophenol is used as a proton donor. Computational studies of the Ni catalyst suggest that non-covalent interactions between the proton donor and ligand heteroatoms are relevant to the mechanism for electrocatalytic HER.

Introduction

Excessive combustion of fossil fuels has resulted in rising average surface temperatures, which has cascading environmental consequences, including melting sea ice, increasingly frequent severe weather events, and significant biodiversity loss, all of which threaten human health, safety, and security.¹ The hydrogen evolution reaction (HER) is an attractive solution for generating carbon-neutral energy, since the dihydrogen (H₂) product can be used directly in fuel cells.² Additionally, HER can be coupled to water oxidation, such that the necessary protons and electrons are supplied from water, an abundant and environmentally benign substrate.^{2,3}

Currently, the best HER electrocatalysts are platinum (Pt)-based, but due to the scarcity and high cost of Pt, more efficient Earth abundant HER catalysts are needed.³ Molecular HER catalysts inspired by hydrogenases have the potential to meet these needs, as Fe-Fe and Fe-Ni hydrogenases are highly active for the HER (turnover frequencies (TOF) = 500-9000 s⁻¹) at or near the thermodynamic potential (<100 mV overpotential).⁴ In recent decades, molecular HER catalysts containing Ni,^{2, 5-7} Fe,⁸ Co,⁹⁻¹² and Mo^{13, 14} active sites have been reported with high selectivity and turnover frequency. Notably, DuBois and coworkers developed Ni bis(diphosphine) complexes with pendent bases as proton relays that have been able to catalyze HER with TOF reaching 106,000 s⁻¹ at an overpotential of 625 mV.⁵⁻⁷ Ni pincer complexes have been shown to operate at lower overpotentials (350-370 mV), but with lower TOF of 209 s⁻¹.⁹ Similarly, cobaloxime derivatives and Co and Ni diamine-dioxime complexes have been shown to be competent HER catalysts at low overpotentials.^{11, 15} Despite these advances, challenges remain in obtaining both low overpotentials and high TOF comparable to hydrogenases, and in generating H₂ from water splitting rather than acids in nonaqueous solvents.^{3,4}

In previous work by our group, first-row molecular transition metal catalysts with 2,2'bipyridine-based N₂O₂ ligand frameworks were shown to be effective for electrocatalytic carbon dioxide (CO₂) reduction¹⁶⁻¹⁹ and O₂ reduction.²⁰⁻²⁴ Based on these studies, we have prepared a less sterically hindered ligand framework, 4-tert-butyl-2-2-[6-[6-(5-tert-butyl-2-hydroxy-phenyl)-2-pyridyl]-2-pyridyl]phenol ($^{p-tbu}$ dhbpy(H)₂). Inspired by previous successes with Ni for CO₂ reduction^{25, 26} and HER catalysts,^{2, 5-7} we prepared the corresponding Ni(II) complex, Ni($^{p-tbu}$ dhbpy). Here we report the synthesis, characterization and electrochemical analysis of Ni($^{p-tbu}$ dhbpy), which serves as an electrocatalyst for the HER. In the presence of pentafluorophenol (C₆F₅OH; estimated p K_a (DMF) = 9.6, see SI), it can generate H₂ with a 94±8% Faradaic efficiency over approximately 9 turnovers at an average TOF of 103±6 s⁻¹ and an overpotential of 1.17 V. DFT calculations reveal favorable hydrogen bonding interactions between the O atoms of the ligand of the Ni catalyst and the C₆F₅OH substrate, identifying a probable key intermediate for the observed electrocatalytic HER.

Experimental Results

The synthetic procedure for ^{p-tbu}dhbpy(H)₂ was similar to a previously reported methodology (see Supporting Information (SI)).^{16, 27} The metalation of the ^{p-tbu}dhbpy(H)₂ ligand was carried out by refluxing in ethanol with sodium acetate and nickel(II) chloride hexahydrate to generate Ni(^{p-tbu}dhbpy) (1) in good yields after work up. The structural assignment of 1 was verified by single-crystal X-ray diffraction studies (**Figure 1**), NMR, UV-vis, ESI-MS (**Figures S4-S6**), and microanalysis.

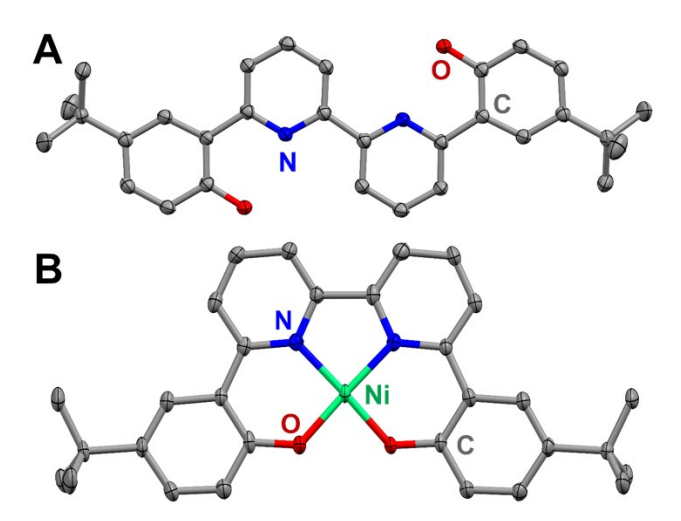


Figure 1. (A) Molecular structure of ^{p-tbu}dhbpy ligand and **(B)** Ni(^{p-tbu}dhbpy) **(1)** obtained from single-crystal X-ray diffraction studies. Blue = N, red = O, gray = C, green = Ni; thermal ellipsoids at 50%, H atoms omitted and occluded MeOH molecule occluded for clarity. CCDC 2155072 and 2155073.

Cyclic voltammetry (CV) studies of **1** under argon (Ar) saturation show that the complex displays a reversible redox features at -1.84 versus Fc⁺/Fc (**Figure 2**, blue). Differential pulse voltammetry (DPV) indicates that the irreversible feature at $E_p = -2.55$ V versus Fc⁺/Fc and the reversible one at -2.69 V versus Fc⁺/Fc correspond to the splitting of a one-electron feature (**Figure S7**). Both are associated with an irreversible oxidation feature at approximately -1.0 V Fc⁺/Fc (**Figure 2**, red). In the presence of pentafluorophenol (F₅C₆OH) as a proton donor under Ar saturation conditions, an increase in current is observed, suggesting that **1** exibits HER activity (**Figure 3**). Additionally, there is an observed positive potential shift in the first reduction feature upon the addition of C₆ F₅OH, which we propose to be suggestive of an interaction of the added proton source with the O atom bound to the metal center. To better probe this interaction, the difference in $E_{1/2}$ with and without C₆ F₅OH present was used to determine the K_{eq} of C₆ F₅OH binding, which was found to be 695 M⁻¹ (assumes 1:1 adduct; Figure S8).^{28, 29}

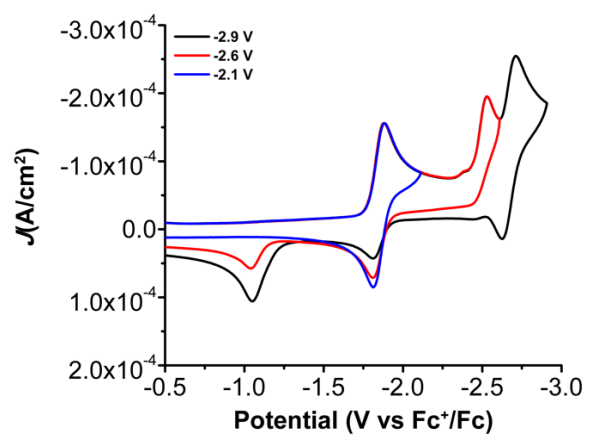


Figure 2. CVs of Ni(^{p-tbu}dhbpy) **1** under Ar saturation at different cut-offs: -2.9 V vs Fc⁺/Fc (black), -2.6 V vs Fc⁺/Fc (red), -2.0 V vs Fc⁺/Fc (blue). Conditions: 1.0 mM analyte in 0.1 M TBAPF₆/DMF; glassy carbon working electrode, glassy carbon rod counter electrode, Ag/AgCl pseudoreference electrode; referenced to Fc⁺/Fc internal standard; 100 mV/s scan rate.

Variable scan rate CVs were taken under Ar saturation and the current density observed at the first reduction feature at -1.84 V vs Fc⁺/Fc was plotted against the square root of the scan rate for scan rates between 25 mV/s and 5000 mV/s (**Figure S9**). In diffusion-controlled and homogenous electrochemical processes, the current density should have a linear relationship with the square root of the scan rate. While the peak cathodic current for the feature at -1.84 V vs Fc⁺/Fc behaved as a homogeneous species, the corresponding oxidation feature deviated slightly from this linear relationship at high scan rates, suggesting that the monoanionic reduction product $[\text{Ni}(p\text{-tbu}dhbpy)]^-$ could be weakly adsorbing to the electrode.

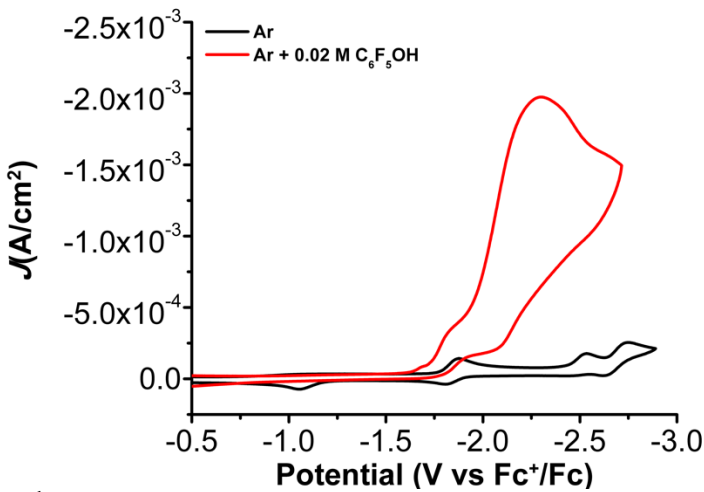


Figure 3. CVs of Ni($^{p-tbu}$ dhbpy) under Ar saturation without C₆F₅OH (black) and with 0.02 M C₆F₅OH (red). Conditions: 1.0 mM analyte in 0.1M TBAPF₆/DMF; glassy carbon working electrode, glassy carbon rod counter electrode, Ag/AgCl pseudoreference electrode; referenced to Fc⁺/Fc internal standard; 100 mV/s scan rate.

To explore the possibility of 1 adsorbing to the electrode, the current at the oxidation peak at $E_p = -1.81 \text{ V}$ vs. Fc^+/Fc is plotted against the scan rate directly. This produced a linear fit of the current density at scan rates higher than 500 mV/s (**Figure S10**), which is consistent with an adsorption process. However, at scan rates from 25-500 mV/s, the peak oxidation current density at $E_p = -1.81 \text{ V}$ vs. Fc^+/Fc still has a linear relationship to the square root of the scan rate (**Figure S9, S11**). This suggests that at faster scan rates (>500 mV/s), complex 1 may be weakly adsorbing to the electrode but remains homogeneous at lower scan rates (25-500 mV/s).

The same variable scan rate experiments were carried out under catalytic conditions (with added C_6F_5OH). The ratio between the peak current under catalytic conditions, i_{cat} , and the peak current under faradaic conditions, i_p , can be related to the maximum turnover frequency (TOF) at each scan rate.³⁰ Under catalytic conditions, the current density plateaued at scan rates above 500 mV/s when plotted against the square root of the scan rate at the second reduction feature, $E_p = -2.33 \text{ V vs Fc}^+/\text{Fc}$ (**Figure S12**). CV data was plotted at scan rates between 25 mV/s and 1000 mV/s to identify if there are regions where catalysis is independent of the scan rate. A plot of the

maximum TOF calculated by i_{cat}/i_p versus the scan rate becomes linear between scan rates of 200 and 500 mV/s (**Figure S13**). TOF_{max} was then calculated for each scan rate from 200-500 mV/s only, to account for the adsorption observed under Faradaic conditions described above (**Table S1**). This resulted in an average TOF_{max} of 103 ± 6 s⁻¹.

Variable concentration CV studies were performed to determine an electrocatalytic rate expression. The logarithm of the current at the second reduction feature, $E_p = -2.33 \text{ V vs Fc}^+/\text{Fc}$, was plotted against the logarithm of added C_6F_5OH for increasing concentrations (**Figure S14**). The resultant correlation between catalytic current density and C_6F_5OH concentration indicates that the electrocatalytic HER is second-order with respect to the C_6F_5OH substrate. The same was done with variable concentration of **1** (**Figure S15**). In this case, a strong correlation between **1** and the observed catalytic current density was not observed, suggesting that the dependence of catalysis on [Ni] is saturated by 0.33 mM.

To establish the homogeneous nature of the electrocatalytic process control CVs were obtained, which showed that the electrode itself could only reduce C₆F₅OH at more negative potentials when the Ni complex was omitted (**Figure S16**). Next, rinse test CVs were performed to examine the degree to which **1** could be adsorbing to the electrode under Faradaic and catalytic conditions at 100 mV/s. CVs in blank solutions without **1** taken immediately after CVs with **1** with and without C₆F₅OH were not significantly different from fresh CVs in identical blank solutions (**Figures S17 and S18**). This further suggests that any adsorption of **1** to the electrode surface is weak at scan rates below 500 mV/s.³¹

Controlled potential electrolysis studies were then performed to determine the product distribution and evaluate catalyst performance for HER. In the presence of 0.05 M C_6F_5OH , the FE for H_2 was $94\pm8\%$ and reached 9.07 ± 0.74 turnovers when the experiment was halted, as

summarized in **Table 1**. H₂ was quantified using the GC calibration curve shown in **Figure S20**. During CPE at –1.9 V vs Fc⁺/Fc the bulk electrolysis trace of the current passed over time displays an induction period (**Figure S21**, **Table S2**). This behavior can be observed when there is a slow transformation from a precatalyst to catalyst species, or when a heterogenized catalytic species accumulates on the electrode surface.³¹ The stability of **1** over the course of electrolysis was analyzed using UV-vis spectroscopy, which showed minimal spectral changes in the key absorbance features between the pre- and post-CPE samples (**Figure S22**). A rinse test CPE was performed to observe possible adsorbed species, generating a small amount H₂ at moderate Faradaic efficiencies (**Figure S23**, **Table S3**). Control CPE experiments with fresh electrodes did not produce enough H₂ to be quantified, suggesting that the H₂ evolution observed in the rinse test was due to minor amounts of an electrode-adsorbed species (**Figure S24**, **Table S4**). While the rinse test showed only a fraction of the H₂ produced in the initial bulk electrolysis, it is clear that some of the observed catalytic activity can be attributed to an electrode-adsorbed species.

Table 1. Summary of CPE data^a

Trial	Atmosphere	$[C_6F_5OH]$ (M)	E _{applied} (V)	TON_{H2}	FE_{H2}
1	Ar	0.05	-2.2	3.17 ± 0.12	75 ± 3
2	Ar	0.05	-1.9	9.07 ± 0.74	94 ± 8
^a Conditions: 1 mM Ni(p-tbu)dhbpy), 0.1M TBAPF ₆ /DMF supporting electrolyte with 0.5 M Fc as sacrificial oxidant.					
Graphite rod working electrode, graphite rod counter electrode, Ag/AgCl pseudoreference electrode.					

Computational Results

With these mechanistic data in hand, computational studies of **1** were done with the Gaussian 16 package at the B3LYP-D3(BJ)/6-311+G(d,p)//B3LYP-D3(BJ)/6-31+G(d,p) level of theory (see **SI** for details). At this level of theory, the calculated reduction potential^{2, 17} of [Ni(P-tbudhbpy)]^{0/1-} of -1.96 V vs Fc⁺/Fc is in reasonable agreement with the experimental value of -1.84 V vs Fc⁺/Fc. Based on an analysis of charge density and KS orbitals, this reduction can be ascribed to a Ni(II)/(I) reduction (**Figures S24** and **S25**). The calculated redox potential for the second

reduction of the four-coordinate complex $[Ni(^{p-tbu}dhbpy)]^{1-}/[Ni(^{p-tbu}dhbpy)]^{2-}$ was found to be -2.65 V vs Fc^+/Fc , which is comparable to the experimental value of $E_p = -2.55 \text{ V}$ vs Fc^+/Fc . Evaluation of the electronic structure of this species was consistent with a ligand-based reduction centered in the bpy-based fragment of the ligand backbone (**Figures S26,S27 and S19**).

A survey of possible ground state optimizations of 1 indicated that the lowest energy spin state was S=0, as expected for a d⁸, square planar Ni(II) complex and in agreement with NMR spectroscopy. Thermodynamic calculations were performed to determine the Gibbs free energy change corresponding to hydrogen-bonding interactions with 1. In the presence of C₆F₅OH, hydrogen bonding interactions with the metal-coordinated oxygen atoms in 1 are predicted to be exothermic by 7.2 kcal/mol. Importantly, the calculated reduction potential for the non-covalent adduct $[Ni(^{p-tbu}dhbpy)(C_6F_5OH)]^0/[Ni(^{p-tbu}dhbpy)(C_6F_5OH)]^{1-}$ shifted to -1.88 V vs Fc^+/Fc (more positive by 80 mV), mirroring the shift observed experimentally (Figure 3 & Figure S8). Conversely, axial DMF coordination to generate [Ni(p-tbu)dhbpy)(DMF)]⁰ is calculated to be endergonic by 3.2 kcal/mol and requires a transition to the S=1 spin surface. Axial DMF coordination to the Ni center is also disfavored when C₆F₅OH engages in a noncovalent interaction with the O atoms of the ligand framework in both the neutral and monoanionic states. In the monoanionic state, we were unable to locate a TS for protonation of the Ni center; further, the protonation of the formally Ni(I) to generate a Ni(III)—H species is predicted to be significantly endergonic (+21.2 kcal/mol). The protonation of a dissociated a phenolate arm to generate the hydrogen-bonded species [Ni(p-tbudhbpy(H))][C₆F₅O)]¹⁻ was found to be 5.3 kcal/mol endergonic, suggesting it was not relevant under protic conditions.

The second reduction of the non-covalent adduct $[Ni(^{p-tbu}dhbpy)(C_6F_5OH)]^{1-}/[Ni(^{p-tbu}dhbpy)(C_6F_5OH)]^{2-}$ is also predicted to undergo a positive shift to $-2.61~V~vs~Fc^+/Fc$, replicating

the shift observed experimentally in **Figure 3** (experimentally $E_p = -2.27 \text{ V}$ with 33 mM C_6F_5OH , positively shifted from $E_p = -2.55 \text{ V}$ at 100 mV/s). From the dianionic species [Ni(p -tbudhbpy)(C_6F_5OH)] $^{2-}$ (S=1), a transition state was located on the potential energy surface (TS +14.6 kcal/mol) and the formation of a hydride was very thermodynamically favorable (-31.1 kcal/mol). Note that for all proton transfers discussed in this paragraph, the given free energies include the contribution expected from homoconjugation of the conjugate base with acid present in solution ($C_6F_5OH = AH$; $AH + A- \rightleftharpoons [AHA]^-$). Protonation of the resulting monoanionic hydride [Ni(H)(p -tbudhbpy)] $^-$ was found to be almost barrierless (TS at +1.2 kcal/mol relative to [Ni(H)(p -tbudhbpy)] $^-$) and exergonic overall (-6.2 kcal/mol) to generate a neutral H_2 adduct. The stepwise release of pentafluorophenolate (as the homoconjugate dimer [($C_6F_5O)_2H$)] $^-$; -24.9 kcal/mol) and H_2 (-5.6 kcal/mol) were both thermodynamically favorable, reforming [Ni(p -tbudhbpy)] 0 0 and completing the catalytic cycle. The overall computed free energy landscape is shown in **Figure 4**.

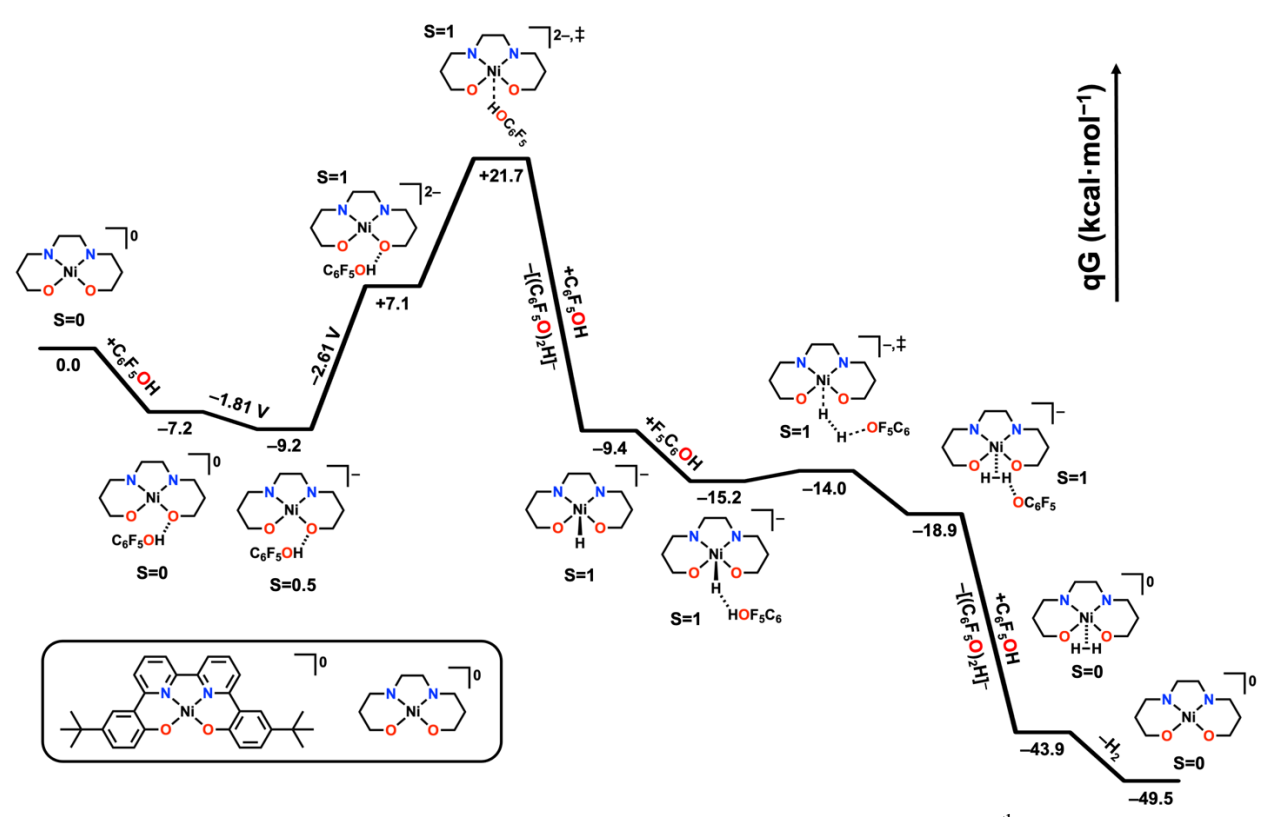


Figure 4. Computed free energy landscape for electrocatalytic HER by $Ni(^{p-tbu}dhbpy)$ (1 mM) in DMF with C_6F_5OH (50 mM) as the proton donor at -1.9 V vs Fc^+/Fc .

As described above, DPV data (**Figure S7**) found that the reversible feature with $E_{1/2} = -2.69 \text{ V}$ vs Fc^+/Fc is part of a split one-electron redox wave coupled to irreversible one observed with $E_p = -2.55 \text{ V}$ versus Fc^+/Fc . This mechanistic proposal is directly supported in variable scan rate studies (**Figure S9**), where the feature at -2.55 V versus Fc^+/Fc becomes more reversible and shows increased current relative to the feature at -2.69 V, indicative that both waves are related to a chemical reaction step (or steps) following one-electron reduction. However, DFT studies exploring the possibilities of partial ligand dissociation and solvent coordination did not generate satisfactory agreement with experiment and uniformly provided reaction pathways which were endergonic with respect to that described in **Figure 4**. The absence of a definitive splitting of the redox wave under catalytic conditions suggests that the hydrogen-bonding interactions help to instead kinetically favor the catalytic cycle proposed above. Indeed, the irreversible oxidation

wave observed at -1.0 V vs Fc⁺/Fc is no longer observed when substrate is present (**Figure 3**), suggesting that the reaction that leads to this splitting under Ar saturation conditions is inhibited during catalysis.

Discussion

Experimental results and computational studies allow a possible mechanism for electrocatalytic HER by 1 to be proposed. Strong hydrogen-bonding interactions between the ligand and the pentafluorophenol proton source generate a non-covalent assembly, [Ni(ptbudhbpy)(C₆F₅OH)]⁰, shifting the first reduction to more positive potentials. The reduction of the resultant monoanionic non-covalent assembly [Ni(p-tbu)dhbpy)(C₆F₅OH)]¹⁻ is also sensitive to the added proton donor and shifts to positive potentials are reflected in the experimental and computational data. The dianion [Ni(p-tbu)dhbpy)(C₆F₅OH)]²⁻ then undergoes protonation at Ni to make a formally Ni(II)-H monoanionic species. Notably, the basicity of the hydride promotes the formation of a H•••H non-covalent interaction with C₆F₅OH, giving rise to [Ni(ptbudhbpy)(H)•••(C₆F₅OH)]¹⁻, from which the barrier to hydride protonation is minimal and forms a Ni(II)-H₂-phenolate adduct following formal proton transfer. Overall, these data suggest that the rate-determining step is the initial protonation and that the resting state of the catalyst is likely to be [Ni(p-tbu)dhbpy)(C₆F₅OH)]¹⁻ during electrolysis at -1.9 V vs Fc⁺/Fc. Although solvent coordination caused a split-wave under Faradaic conditions, compounds which experience phenolate dissociation are predicted to be higher in energy than complexes where the ligand remains four-coordinate.

In general, theory adequately reproduced experimental observations, however, we noted with interest that the difference in calculated and experimental potentials was largest for the one-electron reduction of the monanionic hydrogen-bonded adduct, $[Ni(^{p-tbu}dhbpy)(C_6F_5OH)]^{1-/2-}$,

under catalytic conditions. Given the predicted favorability of C_6F_5OH bonding in all reduction states discussed above, it is likely that additional proton donor interactions occur with the complex in the neutral and reduced states. Although an effective analysis of this type of proton donor clustering effect is beyond the scope of the current study, we were able to identify several possible adducts of with two equivalents of C_6F_5OH (**Figures S28-S30**). Consistent with the proposal that additional proton donor interactions could be occurring which impact the potential of the observed redox waves, the binding of a second equivalent of C_6F_5OH to the unoccupied ligand O atom is exergonic by -6.3 kcal/mol for $[Ni(^{p-tbu}dhbpy)(C_6F_5OH)]^0$ and by -10.5 kcal/mol for $[Ni(^{p-tbu}dhbpy)(C_6F_5OH)]^{1-}$. Finally, additional support is obtained in the predicted $[Ni(^{p-tbu}dhbpy)(C_6F_5OH)_2]^{1-/2-}$ reduction potential of -2.55 V vs Fc^+/Fc , which is 60 mV more positive than that predicted for the monosolvento species.

Conclusions

Bulk electrolysis and CV studies show that the Ni complex described here has a high FE for H_2 generation of $94 \pm 8\%$ with a modest TOF of 103 ± 6 s⁻¹ at an overpotential of 1.17 V. Rinse tests show that some of the active catalyst adsorbs during prolonged electrolysis, but that quantitative selectivity for H_2 is intrinsic to the homogeneous response. The favorable interactions between 1 and C_6F_5OH that precede H_2 formation (positive shifts in the observed reduction potential, favorable binding energies assessed by DFT) suggest that the inclusion of pendent relays could be a route to further improving the activity and stability of this system in future studies. ^{19, 24} Thus, these results introduce a new catalyst design motif that can serve as a platform for the development of new molecular HER catalysts based on abundant transition metals.

ASSOCIATED CONTENT

Supporting Information. Additional CV, UV-vis, NMR, and electrochemical data is included in the SI. This material is available free of charge via the Internet at XXXX. CCDC 2155072-2155073 contain the supplementary crystallographic data for this paper. These data can be obtained free of charge from The Cambridge Crystallographic Data Centre via www.ccdc.cam.ac.uk/structures

AUTHOR INFORMATION

Author Contributions. All authors have given approval to the final version of the manuscript and declare no competing financial interest.

Corresponding Author. * - machan@virginia.edu

Funding Sources

University of Virginia.

ACKNOWLEDGMENT

The authors thank the University of Virginia for generous funding and institutional support, including the use and maintenance of the Rivanna High-Performance Computing system. The National Science Foundation Major Research Instrumentation (CHE 2018870) program funded the X-ray diffractometer. Emma N. Cook is gratefully acknowledged for assistance with the collection of DPV data.

References

- V. Masson- Delmotte, P. Z., H. O. Pörtner, D. Roberts, J. Skea, P.R. Shukla, A. Pirani, W. Moufouma-Okia, C. Péan, R. Pidcock, S. Connors, J. B. R. Matthews, Y. Chen, X. Zhou, M. I. Gomis, E. Lonnoy, T. Maycock, M. Tignor, T. Waterfield (eds.), IPCC, Summary for Policymakers. In: Global warming of 1.5°C. An IPCC Special Report on the impacts of global warming of 1.5°C above pre-industrial levels and related global greenhouse gas emission pathways, in the context of strengthening the global response to the threat of climate change, sustainable development, and efforts to eradicate poverty In Organization, W. M., Ed. Geneva, Switzerland, 2018.
- 2. DuBois, D. L. Development of Molecular Electrocatalysts for Energy Storage. *Inorganic Chemistry* **2014**, 53 (8), 3935-3960 DOI: 10.1021/ic4026969.
- 3. McKone, J. R.; Marinescu, S. C.; Brunschwig, B. S.; Winkler, J. R.; Gray, H. B. Earthabundant hydrogen evolution electrocatalysts. *Chemical Science* **2014**, 5 (3), 865-878 DOI: 10.1039/C3SC51711J.
- 4. Zhang, B.; Sun, L. Artificial photosynthesis: opportunities and challenges of molecular catalysts. *Chemical Society Reviews* **2019**, 48 (7), 2216-2264 DOI: 10.1039/C8CS00897C.
- 5. Wilson, A. D.; Newell, R. H.; McNevin, M. J.; Muckerman, J. T.; Rakowski DuBois, M.; DuBois, D. L. Hydrogen Oxidation and Production Using Nickel-Based Molecular Catalysts with Positioned Proton Relays. *Journal of the American Chemical Society* **2006**, 128 (1), 358-366 DOI: 10.1021/ja056442y.
- 6. Helm, M. L.; Stewart, M. P.; Bullock, R. M.; DuBois, M. R.; DuBois, D. L. A Synthetic Nickel Electrocatalyst with a Turnover Frequency Above 100,000 s<sup>-1</sup> for H<sub>2</sub> Production. *Science* **2011,** 333 (6044), 863 DOI: 10.1126/science.1205864.
- 7. Wilson, A. D.; Shoemaker, R. K.; Miedaner, A.; Muckerman, J. T.; DuBois, D. L.; DuBois, M. R. Nature of hydrogen interactions with Ni(II) complexes containing cyclic phosphine ligands with pendant nitrogen bases. *Proceedings of the National Academy of Sciences* **2007**, 104 (17), 6951 DOI: 10.1073/pnas.0608928104.
- 8. Bhugun, I.; Lexa, D.; Savéant, J.-M. Homogeneous Catalysis of Electrochemical Hydrogen Evolution by Iron(0) Porphyrins. *Journal of the American Chemical Society* **1996**, 118 (16), 3982-3983 DOI: 10.1021/ja954326x.
- 9. Luca, O. R.; Blakemore, J. D.; Konezny, S. J.; Praetorius, J. M.; Schmeier, T. J.; Hunsinger, G. B.; Batista, V. S.; Brudvig, G. W.; Hazari, N.; Crabtree, R. H. Organometallic Ni Pincer Complexes for the Electrocatalytic Production of Hydrogen. *Inorganic Chemistry* **2012**, 51 (16), 8704-8709 DOI: 10.1021/ic300009a.
- 10. Razavet, M.; Artero, V.; Fontecave, M. Proton Electroreduction Catalyzed by Cobaloximes: Functional Models for Hydrogenases. *Inorganic Chemistry* **2005**, 44 (13), 4786-4795 DOI: 10.1021/ic050167z.
- 11. Dempsey, J. L.; Brunschwig, B. S.; Winkler, J. R.; Gray, H. B. Hydrogen Evolution Catalyzed by Cobaloximes. *Accounts of Chemical Research* **2009**, 42 (12), 1995-2004 DOI: 10.1021/ar900253e.
- 12. Hu, X.; Brunschwig, B. S.; Peters, J. C. Electrocatalytic Hydrogen Evolution at Low Overpotentials by Cobalt Macrocyclic Glyoxime and Tetraimine Complexes. *Journal of the American Chemical Society* **2007**, 129 (29), 8988-8998 DOI: 10.1021/ja067876b.
- 13. Garrett, B. R.; Polen, S. M.; Pimplikar, M.; Hadad, C. M.; Wu, Y. Anion-Redox Mechanism of MoO(S2)2(2,2'-bipyridine) for Electrocatalytic Hydrogen Production. *Journal of the American Chemical Society* **2017**, 139 (12), 4342-4345 DOI: 10.1021/jacs.7b01350.

- 14. Karunadasa, H. I.; Chang, C. J.; Long, J. R. A molecular molybdenum-oxo catalyst for generating hydrogen from water. *Nature* **2010**, 464 (7293), 1329-1333 DOI: 10.1038/nature08969.
- 15. Jacques, P.-A.; Artero, V.; Pécaut, J.; Fontecave, M. Cobalt and nickel diimine-dioxime complexes as molecular electrocatalysts for hydrogen evolution with low overvoltages. *Proceedings of the National Academy of Sciences* **2009**, 106 (49), 20627 DOI: 10.1073/pnas.0907775106.
- 16. Hooe, S. L.; Dressel, J. M.; Dickie, D. A.; Machan, C. W. Highly Efficient Electrocatalytic Reduction of CO2 to CO by a Molecular Chromium Complex. *ACS Catalysis* **2019**, 1146-1151 DOI: 10.1021/acscatal.9b04687.
- 17. Moreno, J. J.; Hooe, S. L.; Machan, C. W. DFT Study on the Electrocatalytic Reduction of CO2 to CO by a Molecular Chromium Complex. *Inorganic Chemistry* **2021**, 60 (6), 3635-3650 DOI: 10.1021/acs.inorgchem.0c03136.
- 18. Nichols, A. W.; Chatterjee, S.; Sabat, M.; Machan, C. W. Electrocatalytic Reduction of CO2 to Formate by an Iron Schiff Base Complex. *Inorganic Chemistry* **2018**, 57 (4), 2111-2121 DOI: 10.1021/acs.inorgchem.7b02955.
- 19. Nichols, A. W.; Hooe, S. L.; Kuehner, J. S.; Dickie, D. A.; Machan, C. W. Electrocatalytic CO2 Reduction to Formate with Molecular Fe(III) Complexes Containing Pendent Proton Relays. *Inorg. Chem.* **2020**, 59 (9), 5854-5864 DOI: 10.1021/acs.inorgchem.9b03341.
- Nichols, A. W.; Kuehner, J. S.; Huffman, B. L.; Miedaner, P. R.; Dickie, D. A.; Machan, C. W. Reduction of dioxygen to water by a Co(N2O2) complex with a 2,2'-bipyridine backbone. *Chemical Communications* 2021, 57 (4), 516-519 DOI: 10.1039/D0CC06763F.
- 21. Hooe, S. L.; Rheingold, A. L.; Machan, C. W. Electrocatalytic Reduction of Dioxygen to Hydrogen Peroxide by a Molecular Manganese Complex with a Bipyridine-Containing Schiff Base Ligand. *Journal of the American Chemical Society* **2018**, 140 (9), 3232-3241 DOI: 10.1021/jacs.7b09027.
- 22. Hooe, S. L.; Machan, C. W. Dioxygen Reduction to Hydrogen Peroxide by a Molecular Mn Complex: Mechanistic Divergence between Homogeneous and Heterogeneous Reductants. *Journal of the American Chemical Society* **2019**, 141 (10), 4379-4387 DOI: 10.1021/jacs.8b13373.
- 23. Hooe, S. L.; Cook, E. N.; Reid, A. G.; Machan, C. W. Non-covalent assembly of proton donors and p-benzoquinone anions for co-electrocatalytic reduction of dioxygen. *Chem. Sci.* **2021**, 12 (28), 9733-9741 DOI: 10.1039/D1SC01271A.
- 24. Nichols, A. W.; Cook, E. N.; Gan, Y. J.; Miedaner, P. R.; Dressel, J. M.; Dickie, D. A.; Shafaat, H. S.; Machan, C. W. Pendent Relay Enhances H2O2 Selectivity during Dioxygen Reduction Mediated by Bipyridine-Based Co–N2O2 Complexes. *J. Am. Chem. Soc.* **2021**, 143 (33), 13065-13073 DOI: 10.1021/jacs.1c03381.
- 25. Froehlich, J. D.; Kubiak, C. P. Homogeneous CO2 Reduction by Ni(cyclam) at a Glassy Carbon Electrode. *Inorganic Chemistry* **2012**, 51 (7), 3932-3934 DOI: 10.1021/ic3001619.
- 26. Francke, R.; Schille, B.; Roemelt, M. Homogeneously Catalyzed Electroreduction of Carbon Dioxide—Methods, Mechanisms, and Catalysts. *Chemical Reviews* **2018**, 118 (9), 4631-4701 DOI: 10.1021/acs.chemrev.7b00459.
- 27. Nichols, A. W.; Cook, E. N.; Gan, Y. J.; Miedaner, P. R.; Dressel, J. M.; Dickie, D. A.; Shafaat, H. S.; Machan, C. W. Pendent Relay Enhances H2O2 Selectivity during Dioxygen Reduction Mediated by Bipyridine-Based Co–N2O2 Complexes. *Journal of the American Chemical Society* **2021**, 143 (33), 13065-13073 DOI: 10.1021/jacs.1c03381.
- 28. Gagne, R. R.; Allison, J. L.; Ingle, D. M. Unusual structural and reactivity types for copper(I). Equilibrium constants for the binding of monodentate ligands to several four-coordinate copper(I) complexes. *Inorganic Chemistry* **1979**, 18 (10), 2767-2774 DOI: 10.1021/ic50200a027.

- 29. Nichols, A. W.; Chatterjee, S.; Sabat, M.; Machan, C. W. Electrocatalytic Reduction of CO2 to Formate by an Iron Schiff Base Complex. *Inorg. Chem.* **2018**, 57 (4), 2111-2121 DOI: 10.1021/acs.inorgchem.7b02955.
- 30. Artero, V.; Saveant, J.-M. Toward the rational benchmarking of homogeneous H2-evolving catalysts. *Energy & Environmental Science* **2014,** 7 (11), 3808-3814 DOI: 10.1039/C4EE01709A.
- 31. Lee, K. J.; McCarthy, B. D.; Dempsey, J. L. On decomposition, degradation, and voltammetric deviation: the electrochemist's field guide to identifying precatalyst transformation. *Chemical Society Reviews* **2019**, 48 (11), 2927-2945 DOI: 10.1039/C8CS00851E.

TOC:

Synopsis:

A bipyridine-based Ni complex containing a rigid monoanionic N₂O₂ ligand framework is active for the electrocatalytic hydrogen evolution reaction. Electroanalytical and computational studies support the formation of hydrogen-bonded adducts occurring in all relevant oxidation states, facilitating hydride formation and near barrierless hydride protonation.